



Room Temperature O Transfer from N₂O to CO Mediated by Nearest Cd(I) Ions in MFI Zeolite Cavity

Journal:	<i>Dalton Transactions</i>
Manuscript ID	DT-ART-11-2018-004425.R2
Article Type:	Paper
Date Submitted by the Author:	13-Dec-2018
Complete List of Authors:	Oda, Akira; Okayama University, Department of Chemistry, Graduate School of Natural Science and Technology Ohkubo, Takahiro; Okayama University, Department of Chemistry Kuroda, Yasushige; Okayama Daigaku, Department of Chemistry

Room Temperature O Transfer from N₂O to CO Mediated by Nearest Cd(I) Ions in MFI Zeolite Cavity

Akira Oda,^{1,2*} Takahiro Ohkubo,² Yasushige Kuroda^{2*}

¹Precursory Research for Embryonic Science and Technology, Japan Science and Technology Agency, 4-1-8 Honcho, Kawaguchi, Saitama 332-0012, Japan.

²Department of Chemistry, Graduate School of Natural Science and Technology, Okayama University, 3-1-1 Tsushima, Kita-ku, Okayama 700-8530, Japan.

*Corresponding author. Email: sc19310@s.okayama-u.ac.jp (A.O.); kuroda@cc.okayama-u.ac.jp (Y.K.)

Abstract

The dominant oxidation state of cadmium is +II. Although extensive investigations into the +II oxidation state have been carried out, the chemistry of Cd^I is largely underdeveloped. Here, we report on a new functionality of cadmium created by zeolite lattice: room temperature O transfer from N₂O to CO mediated by the nearest monovalent cadmium ions in MFI zeolite. Thermal activation of Cd^{II} ion-exchanged MFI zeolite in vacuo affords the diamagnetic [Cd^I–Cd^I]²⁺ species with a short Cd^I–Cd^I σ bond (2.67 Å). This species generates two Cd^{I*} sites under UV irradiation through homolytic cleavage of the Cd^I–Cd^I σ bond, and thus-formed nearest Cd^{I*} sites abstract an O atom from N₂O to generate the [Cd^{II}–O–Cd^{II}]²⁺ core. This bridging atomic oxygen species is transferred to CO at room temperature, through which CO oxidation and regeneration of the Cd^I–Cd^I σ bond then proceeds. This is the first example pertaining to the reversible redox reactivity of the nearest monovalent cadmium ions toward stable small molecules. In situ spectroscopic characterization captured all the intermediates in the reaction processes, and these data allowed us to calibrate the density-functional-theory cluster calculations, by which we were able to show that charge compensation requirements from the nearest two Al sites arrayed circumferentially in the 10-membered ring of MFI zeolite create such novel functionalities of cadmium. The unprecedented reactivity of Cd^I and its origin are discussed.

Introduction

The creation of abnormal oxidation states of existing elements has long attracted considerable interest because it has the potential to lead to the development in new chemistries. In this regard, zeolite is one of the attractive materials.

Zeolites are microporous aluminosilicates that are widely used in catalysis and molecular separation–adsorption processes. The well-defined zeolite topology comprises tetrahedral TO_4 units ($\text{T} = \text{Si}^{\text{IV}}$ and Al^{III}). The AlO_4 site has one negative charge due to the substitution of Al^{III} for the more cationic Si^{IV} , thereby forcing the isolated counteranion to be positioned beside the AlO_4 site. Due to the excellent thermal stability of the zeolite framework, such a counteranion is trapped near the AlO_4 site, even at high temperature, and thus, it works effectively as the active site for various types of catalytic reactions.^{1,2} The counteranion can be exchanged with other cations by liquid or solid phase ion-exchange methods, by means of which the properties of zeolites can be tuned.³ Such an Al site has recently been examined as a field to create the long-lived abnormal oxidation states of counteranions under and/or near practical conditions.⁴⁻¹⁸ Recent outstanding examples include single-paramagnetic and dimeric-diamagnetic Cd^{I} species stabilized within the pores of zeolites.^{4,5,14,18}

The dominant oxidation state of cadmium is +II. Although extensive investigations into the +II oxidation state have been carried out, the chemistry of Cd^{I} is largely underdeveloped.¹⁹⁻²² Recently, however, there have been several reports demonstrating that zeolite offers a means to stabilize the monovalent state of cadmium. Seff and coworkers reported the X-ray diffraction analysis of Cd-loaded zeolite, after which they proposed, for the first time, the formation of Cd cluster cations, such as the diamagnetic cadmium(I) dimer species.^{4,5} Wang et al. reported the superior O_2 adsorption property of the paramagnetic Cd^{I} species formed in Cd-loaded zeolite.¹⁴ Morra et al. reported the hyperfine ^{27}Al interactions of Cd^{I} , and elucidated the importance of the Al site in stabilizing the Cd^{I} species.¹⁸

However, many points about the monovalent cadmium in zeolites remain unclear. First, the geometric and electronic structures of the monovalent cadmium species in zeolite are still controversial; spectroscopic assignment and geometrical characterization are inadequate. Second, reactivity studies on Cd^{I} are scarce. To date, only the O_2 activation property of Cd^{I} has been reported.^{14,18} Third, the mechanism of formation of the Cd^{I} species remains unclear. Research carried out in the past indicates that UV irradiation of the Cd-loaded zeolite is essential for preparation of the paramagnetic Cd^{I} species, but neither the role of UV light nor the precursor of the Cd^{I} species has been established experimentally.^{14,18} Thus, it remains unclear why zeolite

creates the abnormal oxidation states of cadmium. Addressing these issues is considered very important, not only for the development in cadmium chemistry, but also for acquiring/understanding new concepts to create abnormal oxidation states of existing elements.

Here, we report on a room temperature O transfer from N₂O to CO mediated by nearest monovalent cadmium ions in MFI zeolite (**Scheme 1**). Thermal activation of a Cd ion-exchanged MFI zeolite affords the diamagnetic [Cd^I-Cd^I]²⁺ species. Under UV irradiation, this species generates two Cd^{I*} sites through the homolytic cleavage of the Cd^I-Cd^I σ bond. The resultant formed Cd^{I*} sites enable O abstraction from N₂O to afford the [Cd^{II}-O-Cd^{II}]²⁺ core. This bridging atomic oxygen species is transferred to CO at room temperature (RT), through which CO oxidation and regeneration of the Cd^I-Cd^I σ bond then proceeds.

In situ spectroscopic characterization captured all the intermediates in the activation processes described in **Scheme 1**. These spectroscopic data allowed us to calibrate the density-functional-theory (DFT) cluster calculations, by which we were able to show that charge compensation requirements from the nearest two Al sites arrayed circumferentially in the 10-membered ring of MFI zeolite create cadmium with new functionalities. The unprecedented reactivity of Cd^I and its origin are discussed.

Experimental methods

Sample preparation. Na ion-exchanged MFI with Si/Al = 11.9 (Tosoh Co; 5 g) was dispersed in 100 mL distilled water containing 0.1 M Cd^{II}(NO₃)₂ (99%; Wako Co.) and stirred at room temperature (RT) for 1 h. The product was collected by centrifugation (4000 rpm) for 10 min and then redispersed in an aqueous solution of Cd^{II}(NO₃)₃. This ion-exchange procedure was repeated 10 times. The ion-exchanged sample was washed by dispersion in 100 mL distilled water at RT for 10 min and then collected by centrifugation (4000 rpm) for 10 min. This procedure was repeated eight times. The resulting sample was then dried overnight at RT under vacuum. The ion-exchange capacity of the prepared sample was determined to be 84%, i.e., Cd^{II}/Al = 0.42, based on a titration method. The obtained Cd ion-exchanged MFI was dehydrated by evacuation at 873 K. This procedure afforded the synthesis of stable [Cd^I-Cd^I]²⁺ species in zeolite pores.

Reactivity assay. A 873 K-evacuated sample was exposed to N₂O (99.9%; GL Sciences Co.) at RT under dark conditions. It was then irradiated with 254 nm light, generated using a 100 W Xe lamp equipped with a 254 nm band pass filter (Asahi Spectra Co.). On completion of the reaction,

the N₂O gas was evacuated at RT. The resulting sample was then exposed to CO (99.9%; GL Sciences Co.) at RT.

In situ X-ray absorption fine structure spectra. The K-edge X-ray absorption fine structure (XAFS) spectra of cadmium, in both the X-ray absorption near edge structure (XANES) and extended XAFS (EXAFS) regions, were collected at the NW10A beamline of the KEK-PF facility (Tsukuba, Japan), which is equipped with a double crystal Si(311) monochromator, under ring operating conditions of 6.5 GeV and 300 mA.

Powdered samples were pressed into pellets (diameter 10 mm, sample weight 100 mg). A pelletized sample was loaded into an in situ cell made of fused silica (available for usage under in situ conditions). XAFS measurements were carried out for the samples evacuated at 873 K. The XANES and EXAFS spectra were recorded at energy intervals of 0.5 eV and 2–3 eV, respectively. The XAFS data were analyzed using software developed by Rigaku Co. For EXAFS analysis, we used the scattering parameters of the reference material, i.e., cadmium(II) oxide (99%, Kanto Chemical Co.).

In situ UV-Vis-NIR diffuse reflectance spectroscopy. The powdered CdMFI sample (100 mg) was placed in a reflectance cell made of fused silica (available for usage under in situ conditions). UV-Vis-NIR diffuse reflectance (DR) spectra were recorded at RT in the wave number range 50000~10000 cm⁻¹ (200~1000 nm) using a spectrophotometer (JASCO V-570) equipped with an integral sphere attachment. Spectralon (Labsphere) was used as the reference material. The resolution was set at 0.5 nm.

In situ electron spin resonance spectroscopy. The powdered sample (5 mg) was loaded into an electron spin resonance (ESR) sample tube (diameter 5 mm). All ESR measurements were carried out in situ. The X-band ESR spectra (ca. 9.0 GHz) were recorded at RT with a JEOL JES-FA200 spectrometer. The *g* values were determined by reference to the ESR spectrum of Mn^{II} doped into MgO as a standard.

Computational methods

DFT cluster calculations were performed using the Gaussian 09 program.²³

Computational characterization of [Cd^I-Cd^I]²⁺ and [Cd^{II}-O_b-Cd^{II}]²⁺ species within the 10-membered ring of MFI zeolite. Following procedures established in previous work,²⁴ we constructed the [Cd₂]²⁺-[Al₂Si₉₀O₁₅₁H₆₆]²⁻ and [Cd₂O]²⁺-[Al₂Si₉₀O₁₅₁H₆₆]²⁻ cluster models having

different Al arrays: the 2NN, 3NN, and 4NN configurations, containing the Al pairs in the second, third, and fourth nearest neighbor positions, respectively, with respect to tetrahedral sites within the 10-membered ring. The Cd–Cd or Cd–O–Cd moieties were positioned around the nearest two Al sites. The coordinates of all atoms were fully optimized. The B3LYP functional was used, with the SDD basis set for Cd, the 6-311G(d,p) basis set for O_b, the 6-31G(d) basis set for the AlO₄ sites, and the 3-21G basis set for other atoms. The total charges in these systems were set to be 0. Ground spin states of the [Cd^I–Cd^I]²⁺ and [Cd^{II}–O–Cd^{II}]²⁺ sites were singlet spin states (*S* = 0). Natural charges of reactive centers were calculated by natural population analyses on the respective fully optimized coordinates. Simulations of the UV-vis spectra of [Cd^I–Cd^I]²⁺ and [Cd^{II}–O_b–Cd^{II}]²⁺ were conducted based on the time-dependent (TD) DFT (TD-DFT) method. Half widths at half maximum of the bands were calculated as 500 cm⁻¹.

Computational evaluation of reactivity of Cd^I–Cd^I/2Cd^I sites toward O transfer from N₂O to CO. The transition states (TSs) were optimized using a TS keyword. The obtained TS geometries were characterized by one imaginary frequency of the vibrational mode relevant to the reaction. The reaction routes, in both the forward and reverse directions, were determined by intrinsic reaction coordinate calculations on the optimized TS geometries. All calculated energies included zero-point energy corrections.

The [Cd^I–Cd^I]²⁺-4NN model was used as the candidate model. This is because the theoretical data of this model compares best with the experimental data. To reduce computational costs regarding the TSs, we used a smaller model truncated from the optimized [Cd^I–Cd^I]²⁺-4NN model. The terminated parts were capped with hydrogen atoms. Optimization was carried out for coordinates of all atoms except the terminated H atoms. Calculations were conducted using the B3LYP functional with the SDD basis set for Cd, the 6-311G(d,p) basis set for CO and N₂O, and the 6-31G(d) basis set for the other atoms.

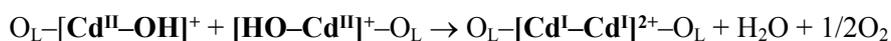
Results and discussion

Cd ion-exchanged MFI zeolite (Si/Al = 11.9, Cd/Al = 0.42) was prepared by a liquid phase ion-exchange method using Cd^{II}(NO₃)₂ as precursor. Hereafter, this sample is denoted as CdMFI. In an effort to prepare the monovalent state of cadmium within the zeolite pore, we induced reduction of the ion-exchanged Cd^{II} species by the activation at 873 K under vacuum—referred to as “autoreduction”.²⁵

The reduction of Cd^{II} was confirmed by X-ray absorption fine structure (XAFS) measurements. **Fig. 1a** shows the X-ray absorption near edge structure (XANES) spectra of CdMFI samples evacuated at 298 K and 873 K. It is evident that higher temperature activation decreases the intensity of the Cd^{II} band at 26716 eV and gives a new broad band in the lower energy region. These changes clearly indicate that the autoreduction of the Cd^{II} species takes place via the activation at 873 K in vacuo.

Fig. 1b shows a comparison of the k^3 -weighted extended XAFS (EXAFS) spectra of CdMFI samples evacuated at 298 K and 873 K, respectively. The sample evacuated at 873 K gives two prominent bands at 1.66 and 2.54 Å (no phase correction). The former band derives from a backscattering from the lattice oxygen atoms ligating with the ion-exchanged cadmium. The latter band derives from a backscattering from the nearest cadmium ion. These assignments were strongly supported by an EXAFS fit able to reproduce the experimental data (**Fig. S1**). The geometrical parameters obtained by the EXAFS fits are summarized in **Table S1**. Of importance here is that the coordination number of Cd for the second shell is almost 1 and the Cd–Cd bond distance is 2.67 Å, which correlates well with the local geometries of previously reported [Cd^I–Cd^I]²⁺ complexes.^{20–22} This correlation suggests formation of the [Cd^I–Cd^I]⁺ species in MFI zeolite. The sample evacuated at 298 K also gives the band attributed to backscattering from the nearest cadmium at 2.72 Å (no phase correction: **Fig. 1b**), but this position is significantly different from that of the 873 K-evacuated sample. EXAFS analysis determined the Cd–Cd distance to be 3.02 Å (**Table S1**), which is longer than that of the 873 K-evacuated sample by ca. 0.4 Å.

These results can be interpreted as follows; the 298 K-evacuated sample contains the nearest Cd^{II} species, such as the nearest Cd^{II}–OH species, and these species decompose to the [Cd^I–Cd^I]²⁺ species via higher temperature activation:



where O_L means the lattice oxygen atoms around the Al atoms. Similar reduction processes have been observed for copper-containing zeolites.^{25,26}

Fig. 2 shows the UV-vis spectra of the CdMFI samples evacuated at 298 K and 873 K. The 873 K-evacuated sample gives three bands with strong intensities in the UV region. Such a spectral feature is not observed for the 298 K-evacuated sample. Therefore, we assigned these bands to the [Cd^I–Cd^I]²⁺ core that is formed via autoreduction of Cd^{II}. A similar spectral feature has also been observed for a homonuclear zinc(I) dimer, [Zn^I–Zn^I]²⁺, in MFI zeolite.¹⁵

To further support the formation of the $[\text{Cd}^{\text{I}}-\text{Cd}^{\text{I}}]^{2+}$ species, we tried to reproduce the obtained experimental data by DFT cluster calculations assuming the presence of the $[\text{Cd}^{\text{I}}-\text{Cd}^{\text{I}}]^{2+}$ species within the zeolite pore. Because the Al positions in the zeolite framework were still unclear, we examined several patterns of Al arrays, i.e., the 2NN, 3NN, and 4NN configurations, containing the Al pairs in the second, third, and fourth nearest neighbor positions, respectively, with respect to tetrahedral sites within the 10-membered ring.²⁴ These Al arrays, which are arrayed circumferentially in the 10-membered ring, have been shown to be good candidate models that qualitatively reproduce the zeolite fields to stabilize the states of nearest monovalent metal ions, divalent metal species, and divalent metal oxide species.^{8,12,15,24,27-35}

We found that all the Al arrays stabilized the state of the $[\text{Cd}^{\text{I}}-\text{Cd}^{\text{I}}]^{2+}$ species and we were able to reproduce the experimental data. As a typical example, **Fig. 3a** shows the optimized geometry of the $[\text{Cd}^{\text{I}}-\text{Cd}^{\text{I}}]^{2+}$ at the 4NN (results of other Al arrays are summarized in **Fig. S2** and **Table S2**). It is evident that the 4NN site stabilizes the ground singlet spin state of the cadmium dimer with a short Cd–Cd bond (2.69 Å). The calculated Cd–Cd bond distance is in good agreement with the EXAFS data (2.67 Å). The natural charges of the two cadmium ions are almost equivalent (+0.72 and +0.74), which indicates the homonuclear $\text{Cd}^{\text{I}}-\text{Cd}^{\text{I}}$ bond. Time-dependent (TD) DFT calculation of such a model qualitatively reproduced the UV-vis spectrum of the 873 K-evacuated CdMFI sample (**Fig. 3b**). Kohn–Sham orbital analysis defined three bands in the UV region as $\sigma \rightarrow \sigma^*$, $\sigma \rightarrow \pi_x$, and $\sigma \rightarrow \pi_y$ transitions of the $[\text{Cd}^{\text{I}}-\text{Cd}^{\text{I}}]^{2+}$ core, having an electronic configuration of $(\sigma)^2(\sigma^*)^0(\pi_x)^0(\pi_y)^0$ (**Fig. 3c**). The correlated results were also obtained from the $[\text{Cd}^{\text{I}}-\text{Cd}^{\text{I}}]^{2+}$ -2NN and -3NN models (**Fig. S2** and **Table S2**). Accordingly, the experimentally calibrated DFT cluster calculations clearly showed the formation of homonuclear cadmium(I) dimer stabilized by the nearest two Al sites arrayed circumferentially in the 10-membered ring of MFI zeolite.

The complexes of $[\text{Cd}^{\text{I}}-\text{Cd}^{\text{I}}]^{2+}$ so far reported were not thermally stable; disproportionation reactions were observed for all complexes below 573 K.²⁰⁻²² It is therefore remarkable that the $[\text{Cd}^{\text{I}}-\text{Cd}^{\text{I}}]^{2+}$ species in MFI zeolite is stable even at 873 K. Such an exceptional stability toward a disproportionation reaction is derived from the charge compensation requirement from the nearest two Al sites that are arrayed circumferentially in the 10-membered ring of MFI zeolite. **Fig. 4** shows the calculated energy profile for the disproportionation reaction at the 4NN site. It can be seen that elimination of Cd atom from the $[\text{Cd}^{\text{I}}-\text{Cd}^{\text{I}}]^{2+}$ -MFI model leads to distortion around one of the AlO_4 sites. This is mainly because of the too long distance for an isolated Cd^{II} ion to achieve the charge balance required from the two Al sites. In contrast to the isolated Cd^{II} ion, the $[\text{Cd}^{\text{I}}-\text{Cd}^{\text{I}}]^{2+}$ state is able to form stable ionic bonds with lattice oxygen atoms around both two Al sites.

Thus, the disproportionation reaction becomes thermodynamically unstable; the disproportionation reaction energy is extremely large: 285 kJ mol⁻¹. Accordingly, the [Cd^I-Cd^I]²⁺ core is forced to be positioned beside the Al sites, even at 873 K. The findings in the present study suggest that the nearest two Al sites arrayed circumferentially in the 10-membered ring of MFI zeolite have potential as a ligand that stabilizes the homonuclear cadmium(I) dimer.

Despite the exceptional stability, the Cd^I-Cd^I σ bond can be activated by photoinduction of the $\sigma \rightarrow \sigma^*$ excitation which leads to reduction of the bond order from 1 to 0. In an effort to understand the reactivity of the nearest monovalent cadmium ions proximately positioned at the 10 membered ring of MFI zeolite, we examined its photoreactivity of the [Cd^I-Cd^I]²⁺ species toward a stable oxidant, i.e., nitrous oxide (N₂O), which has attracted considerable attention recently due to its environmental effects.³⁶ The activation/decomposition of N₂O requires redox active metal sites that induces multiple electron transfers increasing the population of the N₂O- π^* orbital (LUMO), as seen in the nearest Cu^I sites in nitrous oxide reductase and also in Cu-loaded zeolites. Thus, the N₂O activation are rarely known for redox inactive metal such as cadmium. However, the unusually electron rich Cd^I pair sites in MFI zeolite enable two-electron reduction of N₂O. The unprecedented reactivity of cadmium is discussed below.

Fig. 5 shows the UV-vis spectra of the CdMFI sample during the photoactivation in the presence of N₂O. Then, to examine selectively the $\sigma \rightarrow \sigma^*$ excited state reactivity, we used light with a wavelength of 254 nm (approximately corresponding to the $\sigma \rightarrow \sigma^*$ energy gap) (**Fig. S3**). As seen in **Fig. 5**, exposure of the sample to N₂O under dark conditions led to little change in the spectral features of the [Cd^I-Cd^I]²⁺ species; the ground state of the [Cd^I-Cd^I]²⁺ core was not reactive towards N₂O. On the other hand, UV irradiation of the sample in the presence of N₂O gradually caused changes. Spectral features of the [Cd^I-Cd^I]²⁺ species were replaced with new features; intense peaks at 44000, 37000, and 31000 cm⁻¹ emerged. Finally, the spectroscopic features of the [Cd^I-Cd^I]²⁺ species completely disappeared. In this reaction, the formation of N₂ was also confirmed by mass measurement. These results suggest the O transfer from N₂O to the [Cd^I-Cd^I]²⁺ species with the formation of the [Cd^{II}-O_b-Cd^{II}]²⁺ core, where O_b means the oxygen atom bridging two cadmium ions. Analogous reactions have also been observed on the nearest monovalent copper sites in zeolites.^{29,32}

To support the formation of the [Cd^{II}-O_b-Cd^{II}]²⁺ core, its spectroscopic features were computationally examined. **Fig. 6a** shows the optimized [Cd^{II}-O_b-Cd^{II}]²⁺-MFI model containing an Al pair with the 4NN configuration (results of other Al arrays are given in **Table S3** and **Fig. S4**). The [Cd^{II}-O_b-Cd^{II}]²⁺ model was constructed by the addition of an oxygen atom into the [Cd^I-

$\text{Cd}^{\text{I}}\text{]}^{2+}$ -MFI model shown in **Fig. 3a**. The O addition leads to elongation of the Cd–Cd distance from 2.69 Å to 3.60 Å and generates a ground singlet spin state of a bent core of Cd–O_b–Cd (128°). The natural charges of respective cadmium ions increase by ca. 0.6 from the original $[\text{Cd}^{\text{I}}\text{–Cd}^{\text{I}}]^{2+}$ state. The natural charge of O_b is –1.2, which indicates that the bridged oxo species donates ca. 0.8e to the nearest cadmium ions, thereby creating stable acid–base bonds with cadmium ions. On these grounds, we defined this model as the mono(μ -oxo)dicadmium(II) site. The TD-DFT calculation of such a model qualitatively reproduces the experimental data (**Fig. 6b**). All the bands derive from the excitations from O_b-2p orbitals to Cd-5s orbitals, as shown in **Fig. 6c**. Similar results were also observed for the 2NN and 3NN models (**Table S3** and **Fig. S4**). The obtained correlation between experiment and theory clearly shows the formation of the $[\text{Cd}^{\text{II}}\text{–O}_b\text{–Cd}^{\text{II}}]^{2+}$ species via photoreaction of the Cd^I–Cd^I σ bond with N₂O. It is noteworthy that this is the first example of the identification of the μ -oxo complex of cadmium.

In situ electron spin resonance (ESR) measurement captured the intermediate species in the reaction with N₂O. **Fig. 7** shows the ESR spectra for the CdMFI sample before and after irradiation with 254 nm light under vacuum and subsequent exposure to N₂O at RT. Prior to UV irradiation, the sample exhibits only a low intensity peak at around center field, which derives from defects in the zeolite framework. On the other hand, the UV-irradiated sample shows an axial ESR signal at around $g = 1.993$ and the hyperfine structures of ¹¹¹Cd and ¹¹³Cd ($I = 1/2$, 12.8% and 12.22% natural abundances) in the higher magnetic field. These ESR signals are stable under vacuum. According to recent work of Morra et al., these spectral features derive from the paramagnetic Cd^{I*} (4d¹⁰ 5s¹) species anchored on the Al site in MFI zeolite.¹⁸ The formation of the Cd^{I*} species in the present system can be interpreted by considering the homolytic cleavage of the Cd^I–Cd^I σ bond via photoinduction of the $\sigma \rightarrow \sigma^*$ transition (**Scheme 1, A→B**). Similar phenomenon was also observed in $[\text{Zn}^{\text{I}}\text{–Zn}^{\text{I}}]^{2+}$ -containing zeolites.^{15,34} The formed Cd^{I*} species is highly reactive due to its opened electronic structure. Subsequent N₂O treatment of the photoactivated CdMFI sample leads to the disappearance of the spectral features of Cd^{I*}, where no additional ESR signal is observed. These data indicate that the Cd^{I*} species converts to the ESR silent species, i.e., the $[\text{Cd}^{\text{II}}\text{–O}_b\text{–Cd}^{\text{II}}]^{2+}$ species, through an O abstraction from N₂O (**Scheme 1, B→C**).

To obtain mechanistic insights, the reactivity of the nearest two Cd^{I*} sites toward O abstraction from N₂O was evaluated computationally. **Fig. 8** shows the potential energy surface of the O abstraction from N₂O by the photoactivated $[\text{Cd}^{\text{I}}\text{–Cd}^{\text{I}}]^{2+}$ species at the nearest two Al sites with the 4NN configuration (geometrical details are given in **Fig. S5**). For the ground singlet

spin state of the N_2O adsorbed on the $[\text{Cd}^{\text{I}}-\text{Cd}^{\text{I}}]^{2+}$ core (**model a**), N_2O weakly interacts with one of the cadmium ions; thus, the $\text{Cd}^{\text{I}}-\text{Cd}^{\text{I}}$ bond is hardly changed from the original state (2.67 Å). However, an optimization of the excited triplet spin state assuming a $\sigma \rightarrow \sigma^*$ excitation leads to an elongation of the $\text{Cd}^{\text{I}}-\text{Cd}^{\text{I}}$ bond to 4.08 Å (**model b**). In the optimized triplet spin state, almost all spin densities are localized on the 5s orbitals of two cadmium ions (see blue surfaces in **Fig. 8**). This indicates the formation of the nearest two Cd^{I} sites: $(4d)^{10}(5s)^1$ metallo-radical pair. The calculated spin densities are 0.87e and 0.88e for the respective cadmium ions, which correlates well with an experimental value (0.84e) obtained by the ^{111}Cd **A** tensor for the Cd^{I} species formed in the photoactivated Cd-containing MFI zeolite.¹⁸ The residual spin densities (0.25e) are localized on the lattice oxygen atoms around the Al sites, as previously indicated by Morra et al.¹⁸ Next, the N_2O molecule approaches one of the two Cd^{I} ions via an O end, and then the spin density of Cd^{I} partially transfers to an unoccupied $\text{N}_2\text{O}-\pi^*$ orbital (**model TS_{b-c}**). This electron transfer facilitates the O abstraction from N_2O to generate both a N_2 molecule and the highly reactive $[\text{Cd}^{\text{II}}-\text{O}^{\cdot}]^+$ species that weakly interacts with the neighboring monovalent cadmium ion (**model c**). The N-end approach mechanism was not found in the present case, which indicates the low affinity of Cd^{I} toward Cd–N bond formation. Finally, a radical coupling takes place between the $[\text{Cd}^{\text{II}}-\text{O}^{\cdot}]^+$ species and the neighboring Cd^{I} ion, resulting in the formation of a ground singlet spin state of the $[\text{Cd}^{\text{II}}-\text{O}_b-\text{Cd}^{\text{II}}]^{2+}$ core (**model d**). This final product is more stable than the initial state by 136 kJ mol⁻¹. The rate-determining step is **TS_{b-c}** and its activation barrier is only 37 kJ mol⁻¹. These data clearly indicate the high reactivity of the nearest two Cd^{I} sites toward the O abstraction from N_2O , which is consistent with experimental results.

Taking accounts of the redox potential of cadmium, it seems that the $[\text{Cd}^{\text{II}}-\text{O}_b-\text{Cd}^{\text{II}}]^{2+}$ core is not reactive toward oxidative reactions. However, it was found unexpectedly that the $[\text{Cd}^{\text{II}}-\text{O}_b-\text{Cd}^{\text{II}}]^{2+}$ species newly found in the present study is highly reactive toward the CO oxidation reaction.³⁷ **Fig. 9** shows UV-vis spectra of the $[\text{Cd}^{\text{II}}-\text{O}_b-\text{Cd}^{\text{II}}]^{2+}$ -containing sample upon reaction with CO. After RT exposure of the sample to CO, the spectral features of the $[\text{Cd}^{\text{II}}-\text{O}_b-\text{Cd}^{\text{II}}]^{2+}$ core are replaced with those of the $[\text{Cd}^{\text{I}}-\text{Cd}^{\text{I}}]^{2+}$ species. The original spectrum of the $[\text{Cd}^{\text{I}}-\text{Cd}^{\text{I}}]^{2+}$ species is recovered. Furthermore, CO_2 was definitely detected by mass measurement. These results clearly indicate the RT O transfer from the $[\text{Cd}^{\text{II}}-\text{O}_b-\text{Cd}^{\text{II}}]^{2+}$ species to CO with the regeneration of the $[\text{Cd}^{\text{I}}-\text{Cd}^{\text{I}}]^{2+}$ core (**Scheme 1, C→A**).

Our claim was substantiated by computational evaluation of the reactivity of the $[\text{Cd}^{\text{II}}-\text{O}_b-\text{Cd}^{\text{II}}]^{2+}$ core toward CO oxidation. **Fig. 10** shows the potential energy surface of the CO oxidation mediated by the $[\text{Cd}^{\text{II}}-\text{O}_b-\text{Cd}^{\text{II}}]^{2+}$ -4NN site (geometrical details are given in **Fig. S6**). First, the

CO molecule weakly interacts with one of the cadmium ions (**model e**). Second, the CO molecule approaches the O_b via TS_{e-f} , resulting in the formation of the $[Cd^{II}-(CO_2)-Cd^{II}]^{2+}$ species (**model f**). Third, the inserted CO_2 adduct moves outside via TS_{f-g} , resulting in the formation of the CO_2 species bound to two cadmium ions in a side-on fashion (**model g**). Finally, the CO_2 species is released as the linear CO_2 molecule via TS_{g-h} , resulting in the regeneration of the Cd^I-Cd^I σ bond (**model h**). This sequential geometrical change correlates well with the analogous reaction mediated by homonuclear Ge-Ge complexes.³⁸ The rate-determining step in our system is TS_{e-f} , i.e., the O_b-CO bond formation process. This process requires an activation barrier of only 48 kJ mol⁻¹. Reaction enthalpy is highly stabilized in the product: -217 kJ mol⁻¹. The calculated low activation energy as well as high reaction enthalpy are consistent with the experimentally observed RT reactivity of the $[Cd^{II}-O_b-Cd^{II}]^{2+}$ core toward the CO oxidation.

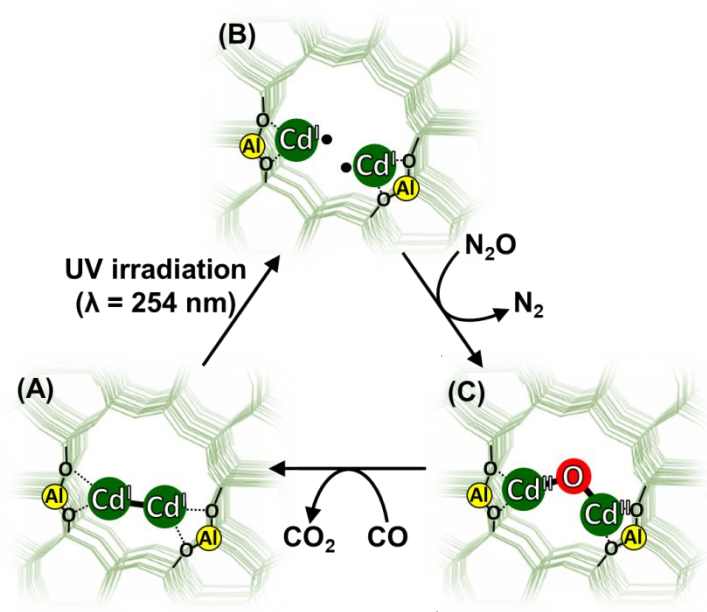
It is noteworthy that this is the first example pertaining to reversible redox reactivity of nearest monovalent cadmium ions toward stable small molecules. Needless to say, the exceptional stability of the Cd^I-Cd^I bond, created by the nearest two Al sites arrayed circumferentially in the 10-membered ring of MFI zeolite, contributes to this reversible reactivity. Our findings suggest that the nearest two Al sites arrayed circumferentially in the 10-membered ring of MFI zeolite have potential as a ligand that creates new functionalities of abnormal oxidation states of metal ions.

Conclusions

In summary, the present study has revealed the exceptional reactivity of enclosed monovalent cadmium ions, i.e., the $[Cd^I-Cd^I]^{2+}$ core and the nearest two Cd^I sites, toward O transfer from N_2O to CO (**Scheme 1**).

The $[Cd^I-Cd^I]^{2+}$ species is formed in Cd-containing MFI zeolite by thermal activation at 873 K under vacuum. The short Cd^I-Cd^I σ bond (2.67 Å) was detected by EXAFS analysis. This species shows distinct absorption bands in the UV region. These bands are derived from the excitations from a doubly occupied Cd^I-Cd^I σ bonding orbital to empty σ^* , π_x , and π_y orbitals. The photoinduction of the $\sigma \rightarrow \sigma^*$ excitation leads to homolytic cleavage of the Cd^I-Cd^I σ bond, which results in the formation of the nearest two Cd^I radicals. The enclosed metallo-radicals enable the O abstraction from N_2O to afford the $[Cd^{II}-O_b-Cd^{II}]^{2+}$ core. The resultant formed bridging atomic oxygen species is transferred to CO at RT, through which CO oxidation and regeneration of the Cd^I-Cd^I σ bond takes place. This is the first example pertaining to the reversible reactivity of the

nearest monovalent cadmium ions toward stable small molecules. The experimentally calibrated DFT calculations allowed us to visualize the Al array, which is essential for the creation of new functionalities of the nearest monovalent cadmium ions. Subsequently, we were able to show that the nearest two Al sites arrayed circumferentially in the 10-membered ring of MFI zeolite have potential as a ligand that creates the new functionalities of abnormal oxidation states of metal ions.



Scheme 1 Novel reactions found in the $[\text{Cd}^{\text{I}}-\text{Cd}^{\text{I}}]^{2+}$ -MFI system: room temperature O transfer from N_2O to CO mediated by the nearest Cd^{I} ions in MFI zeolite.

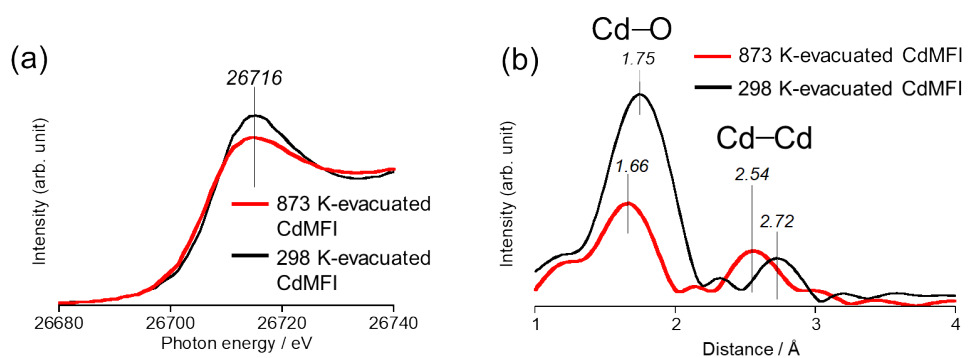


Fig. 1 (a) XANES and (b) k^3 -weighted EXAFS spectra ($2 < k < 12 \text{ \AA}^{-1}$) of CdMFI samples evacuated at 298 K (black line) and 873 K (red line), respectively.

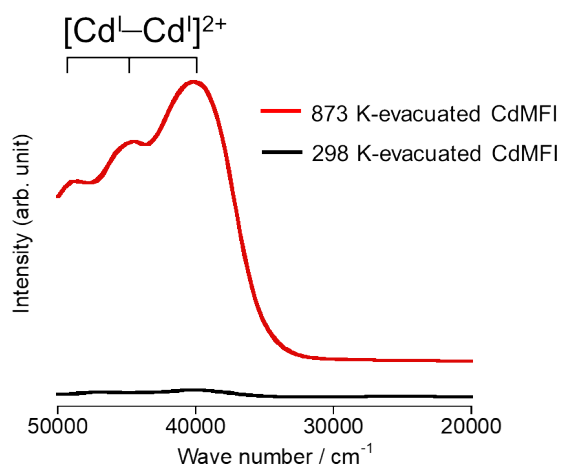


Fig. 2 UV-vis diffuse reflectance spectra of CdMFI samples evacuated at 298 K (black line) and 873 K (red line). respectively.

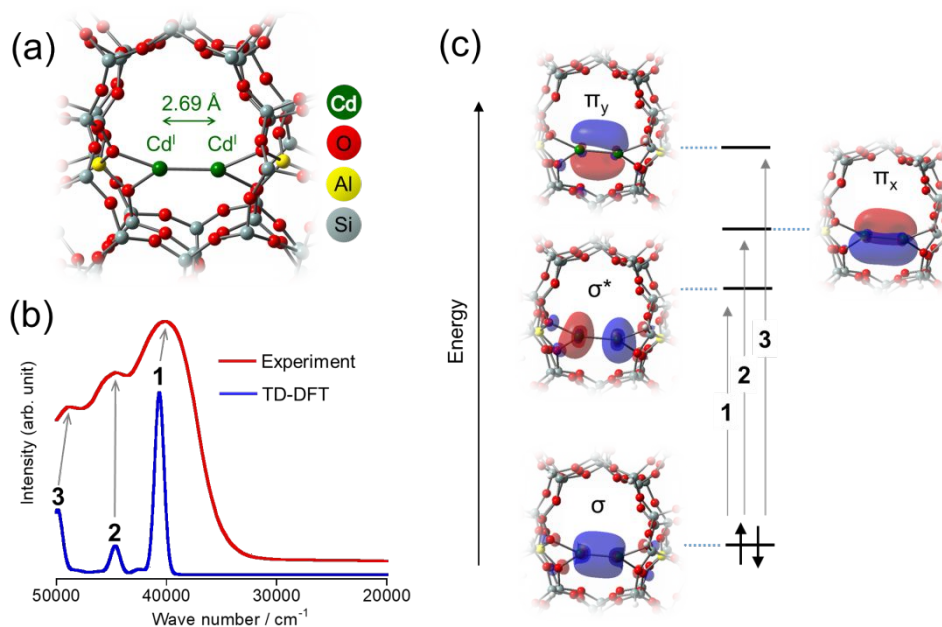


Fig. 3 (a) Optimized [Cd^I-Cd^I]²⁺-MFI model containing an Al pair in the fourth nearest neighbor positions within the 10-membered ring of MFI zeolite. (b) Comparison of the TD-DFT result with the UV-vis diffuse reflectance spectrum of the 873 K-evacuated CdMFI sample. (c) Kohn-Sham orbitals involved in the respective excitations 1–3.

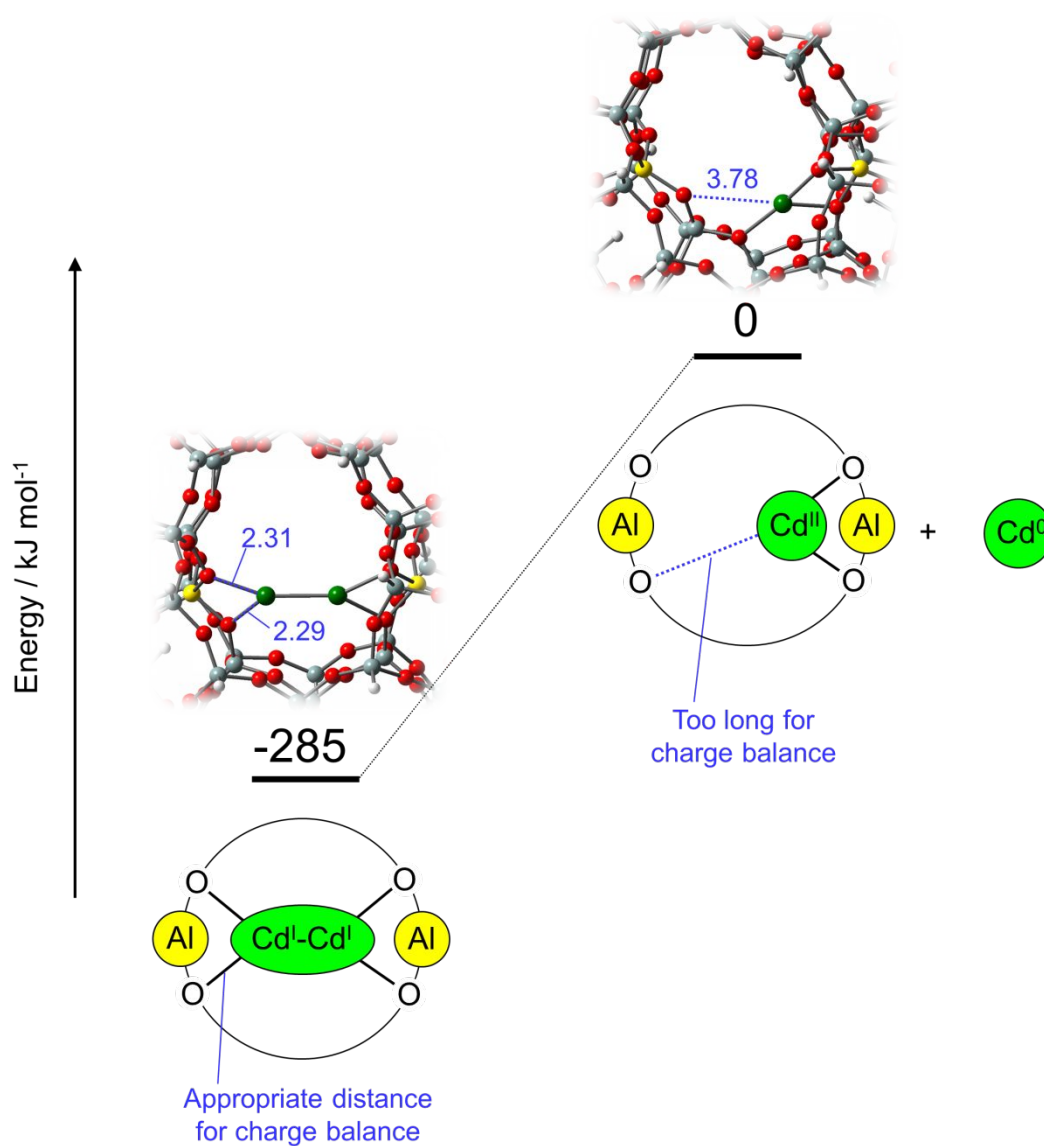


Fig. 4 Energy profile for the disproportionation reaction of $[\text{Cd}^{\text{I}}-\text{Cd}^{\text{I}}]^{2+}$ to Cd^{II} and Cd^0 at the 4NN site. Schematics of models and fully optimized clusters are also shown. Relative energies are given as black numbers. The selected distances between lattice oxygen atoms and cadmium ions are included in the figures as blue numbers (\AA). Similar disproportionation reaction energies were obtained for the 2NN and 3NN sites: 271 kJ mol^{-1} and 269 kJ mol^{-1} , respectively.

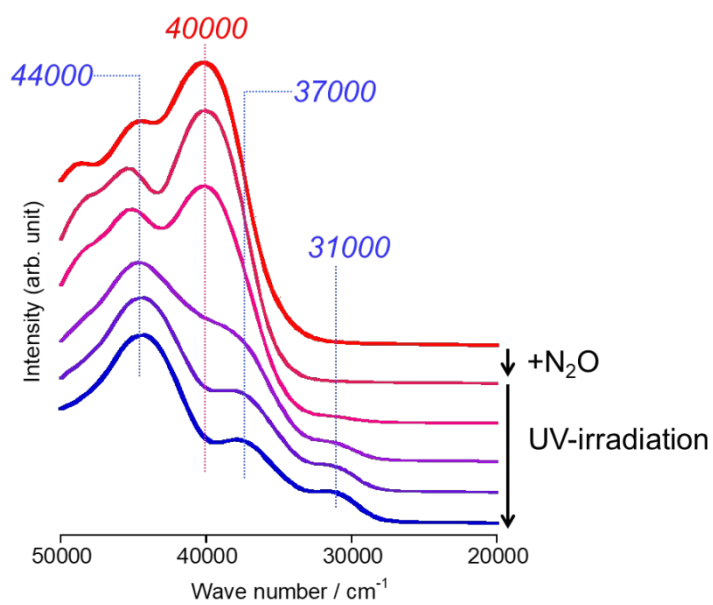


Fig. 5 Change in UV-vis diffuse reflectance spectra of the CdMFI sample upon 254 nm UV irradiation in the presence of N₂O.

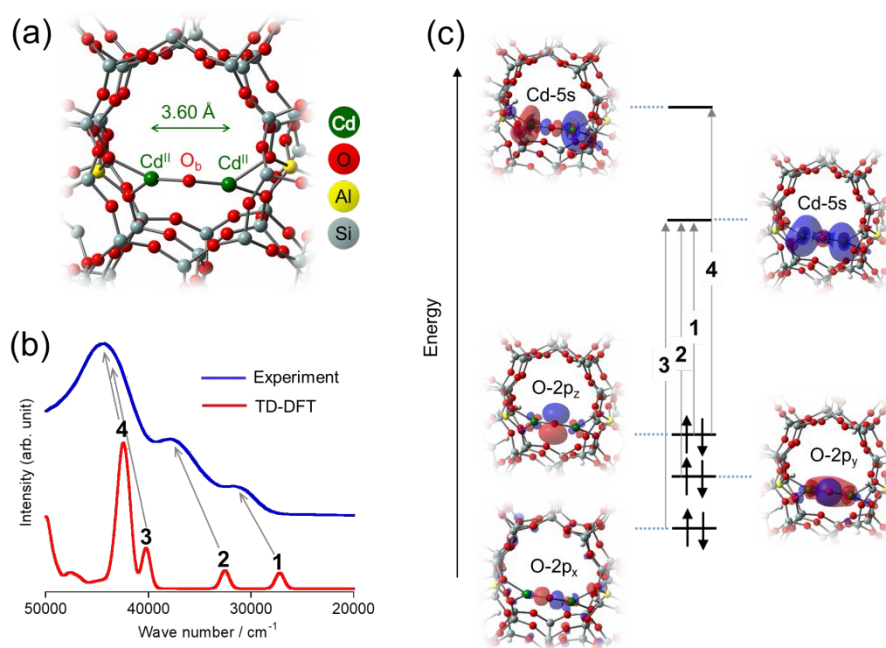


Fig. 6 (a) Optimized $[Cd^{II}-O_6-Cd^{II}]^{2+}$ -4NN model. (b) A comparison of the TD-DFT result with the UV-vis diffuse reflectance spectrum of the CdMFI sample after photoreaction with N_2O . (c) Kohn-Sham orbitals involved in the respective excitations 1–4.

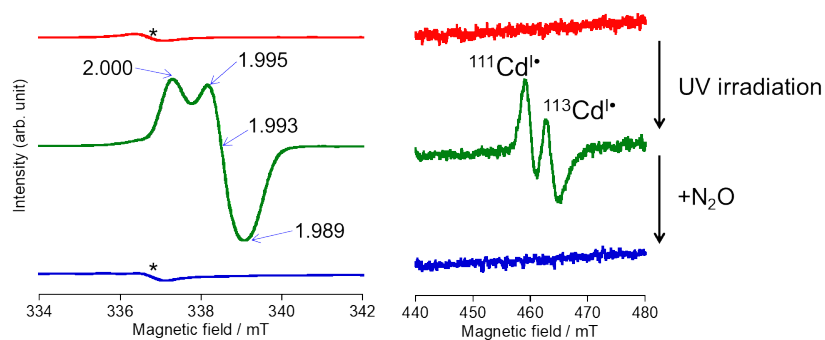


Fig. 7 In situ ESR spectroscopic characterization of the intermediates in the photoreaction of the $[\text{Cd}^{\text{I}}-\text{Cd}^{\text{I}}]^{2+}$ species with N_2O : (red line) sample before UV irradiation; (green line) sample after 254 nm UV irradiation under vacuum; (blue line) sample after 254 nm UV irradiation under vacuum and subsequent RT treatment with N_2O . Asterisk indicates the ESR signal attributed to zeolite defects that are formed in the pretreatment process.

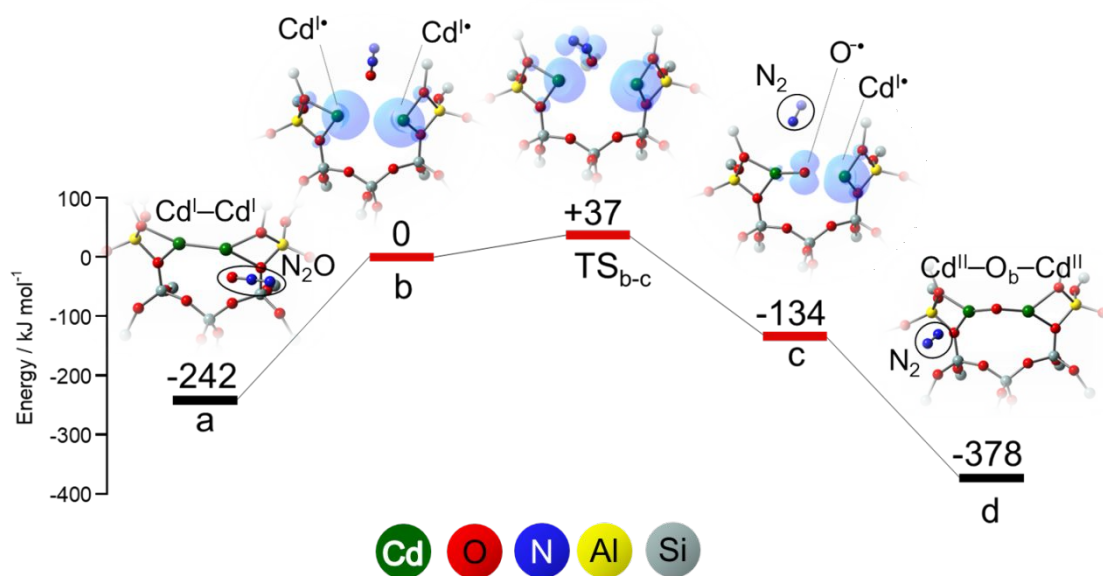


Fig. 8 Zero-point energy-corrected potential energy surface of the O abstraction from N_2O by the photoactivated $[\text{Cd}^{\text{I}}-\text{Cd}^{\text{I}}]^{2+}$ species sitting at the 4NN site. This reaction involves the singlet and triplet spin states of the $[\text{Cd}^{\text{I}}-\text{Cd}^{\text{I}}]^{2+}$ species. Energies of the singlet spin states are given as black bars and energies of the triplet spin states are given as red bars. The calculated energies relative to the model b are given as black numbers. Corresponding models are also shown, where spin densities of the triplet state models are described as blue surfaces.

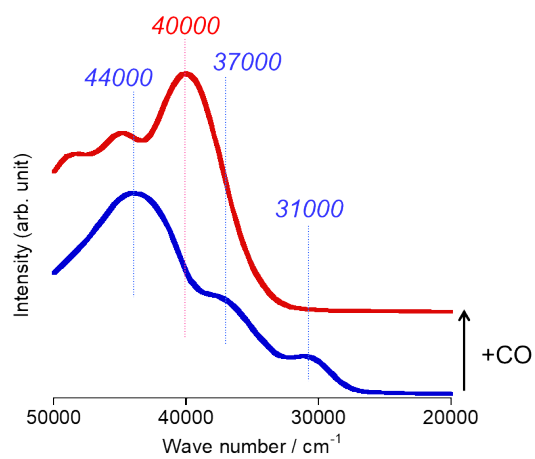


Fig. 9 UV-vis spectra of the CO oxidation by the N₂O-activated CdMFI sample at RT.

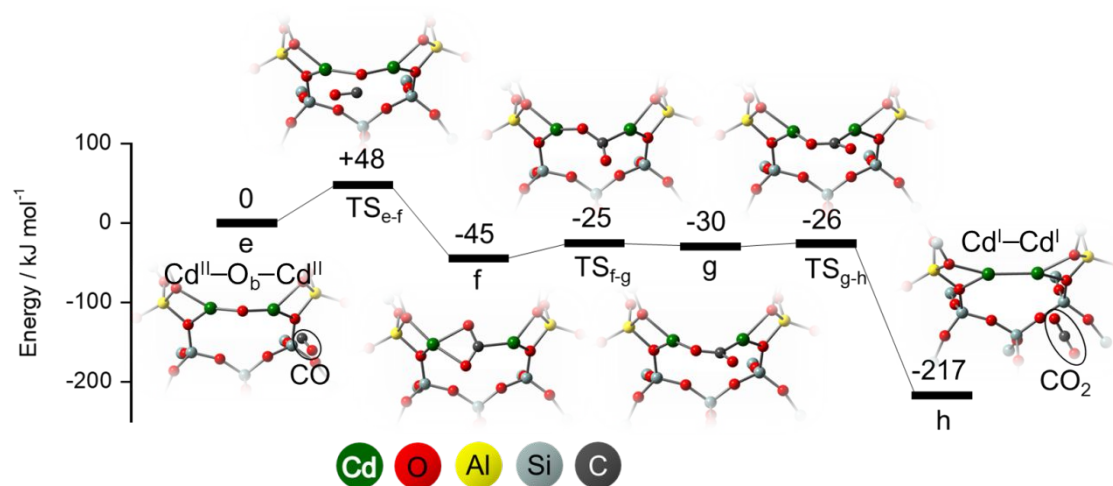


Fig. 10 Zero-point energy-corrected potential energy surface of the CO oxidation mediated by the [Cd^{II}-O_b-Cd^{II}]²⁺ core sitting at the 4NN site. The calculated energy relative to model e is given as black numbers. Optimized geometries of the respective steps are also shown. As the excited triplet spin state is significantly higher in energy than the ground singlet spin state, this reaction takes place only on the ground singlet spin surface; the triple spin state offers no contribution to the respective steps.

Acknowledgements

A.O. acknowledges supports from the Japan Society for the Promotion of Science (Research Fellowship for Young Scientists, DC1 and PD) and from the Japan Science and Technology Agency.

References and Note

- (1) T. Yokoi, H. Mochizuki, S. Namba, J. N. Kondo and T. Tatsumi, *J. Phys. Chem. C* 2015, **119**, 15303–15315.
- (2) M. Yoshioka, T. Yokoi and T. Tatsumi, *ACS Catal.* 2015, **5**, 4268–4275.
- (3) M. Iwamoto and H. Yahiro, *Catal. Today* 1994, **22**, 5–18.
- (4) L. B. Mccusker and K. Seff, *J. Am. Chem. Soc.* 1979, **101**, 5235–5239.
- (5) S. B. Jang, U. S. Kim, Y. Kim and K. Seff, *J. Phys. Chem.* 1994, **98**, 3796–3800.
- (6) L. Li, G. D. Li, C. Yan, X. Y. Mu, X. L. Pan, X. X. Zou, K. X. Wang and J. S. Chen, *Angew. Chem. Int. Ed.* 2011, **50**, 8299–8303.
- (7) P. Pietrzyk, K. Podolska, T. Mazur and Z. Sojka, *J. Am. Chem. Soc.* 2011, **133**, 19931–19943.
- (8) A. Oda, H. Torigoe, A. Itadani, T. Ohkubo, T. Yumura, H. Kobayashi and Y. Kuroda, *Angew. Chem. Int. Ed.* 2012, **51**, 7719–7723.
- (9) X. Wang, G. Qi, J. Xu, J. B. Li, C. Wang and F. Deng, *Angew. Chem. Int. Ed.* 2012, **51**, 3850–3853.
- (10) P. Pietrzyk, T. Mazur, K. Podolska-Serafin, M. Chiesa and Z. Sojka, *J. Am. Chem. Soc.* 2013, **135**, 15467–15478.
- (11) G. Qi, J. Xu, J. Su, J. Chen, X. Wang and F. Deng, *J. Am. Chem. Soc.* 2013, **135**, 6762–6765.
- (12) A. Oda, H. Torigoe, A. Itadani, T. Ohkubo, T. Yumura, H. Kobayashi and Y. Kuroda, *J. Am. Chem. Soc.* 2013, **135**, 18481–18489.
- (13) D. Seoung, Y. Lee, H. Cynn, C. Park, K. Y. Choi, D. A. Blom, W. J. Evans, C. C. Kao, T. Vogt and Y. Lee, *Nat. Chem.* 2014, **6**, 835–839.
- (14) J.-F. Wang, D. Wang, H. Zeng and Z.-F. Zhou, *RSC Adv.* 2015, **5**, 77490–77494.
- (15) A. Oda, T. Ohkubo, T. Yumura, H. Kobayashi and Y. Kuroda, *Dalton Trans.* 2015, **44**, 10038–10047.
- (16) A. Oda, T. Ohkubo, T. Yumura, H. Kobayashi and Y. Kuroda, *Angew. Chem. Int. Ed.* 2017, **56**, 9715–9718.

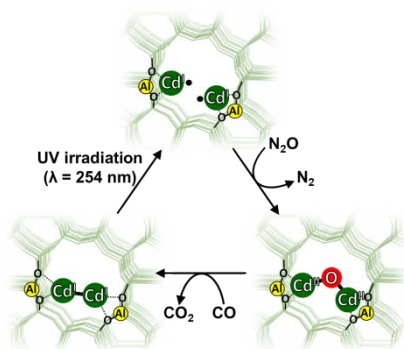
- (17) E. Morra, G. Berlier, E. Borfecchia, S. Bordiga, P. Beato and M. Chiesa, *J. Phys. Chem. C* 2017, **121**, 14238–14245.
- (18) E. Morra and M. Chiesa, *J. Phys. Chem. C* 2018, **122**, 9515–9522.
- (19) D. L. Reger, S. S. Mason and A. L. Rheingold, *J. Am. Chem. Soc.* 1994, **116**, 2233–2233.
- (20) Z. Zhu, R. C. Fischer, J. C. Fettinger, E. Rivard, M. Brynda and P. P. Power, *J. Am. Chem. Soc.* 2006, **128**, 15068–15069.
- (21) Z. Zhu, M. Brynda, R. J. Wright, R. C. Fischer, W. A. Merrill, E. Rivard, R. Wolf, J. C. Fettinger, M. M. Olmstead and P. P. Power, *J. Am. Chem. Soc.* 2007, **129**, 10847–10857.
- (22) E. Carmona and A. Galindo, *A. Angew. Chem. Int. Ed.* 2008, **47**, 6526–6536.
- (23) M. Frisch, G. Trucks, H. Schlegel, G. Scuseria, M. Robb, J. Cheeseman, G. Scalmani, V. Barone, B. Mennucci and G. Petersson, Gaussian 09, Revision A. 02; Gaussian, Inc: Wallingford, CT, 2009.
- (24) T. Yumura, M. Takeuchi, H. Kobayashi and Y. Kuroda, *Inorg. Chem.* 2009, **48**, 508–517.
- (25) B. E. R. Snyder, M. L. Bols, R. A. Schoonheydt, B. F. Sels and E. I. Solomon, *Chem. Rev.* 2018, **118**, 2718–2768.
- (26) Y. Kuroda, Y. Yoshikawa, S. Konno, H. Hamano, H. Maeda, R. Kumashiro and M. Nagao, *J. Phys. Chem.* 1995, **99**, 10621–10628.
- (27) T. Yumura, T. Nanba, H. Torigoe, Y. Kuroda and H. Kobayashi, *Inorg. Chem.* 2011, **50**, 6533–6542.
- (28) A. Itadani, H. Torigoe, T. Yumura, T. Ohkubo, H. Kobayashi and Y. Kuroda, *J. Phys. Chem. C* 2012, **116**, 10680–10691.
- (29) M. L. Tsai, R. G. Hadt, P. Vanelderen, B. F. Sels, R. A. Schoonheydt and E. I. Solomon, *J. Am. Chem. Soc.* 2014, **136**, 3522–3529.
- (30) T. Yumura, A. Oda, H. Torigoe, A. Itadani, Y. Kuroda, T. Wakasugi and H. Kobayashi, *J. Phys. Chem. C* 2014, **118**, 23874–23887.
- (31) J. Gao, Y. Zheng, J. M. Jehng, Y. Tang, I. E. Wachs and S. G. Podkolzin, *Science* 2015, **348**, 686–690.
- (32) P. Vanelderen, B. E. Snyder, M. L. Tsai, R. G. Hadt, J. Vancauwenbergh, O. Coussens, R. A. Schoonheydt, B. F. Sels and E. I. Solomon, *J. Am. Chem. Soc.* 2015, **137**, 6383–6392.
- (33) A. Itadani, Y. Sogawa, A. Oda, T. Ohkubo, T. Yumura, H. Kobayashi, M. Sato and Y. Kuroda, *J. Phys. Chem. C* 2015, **119**, 21483–21496.
- (34) L. Benco, *J. Phys. Chem. C* 2016, **120**, 6031–6038.
- (35) A. Oda, T. Ohkubo, T. Yumura, H. Kobayashi and Y. Kuroda, *Phys. Chem. Chem. Phys.* 2017, **19**, 25105–25114.

(36) W. B. Tolman, *Angew. Chem. Int. Ed.* 2010, **49**, 1018-1024.

(37) In the present study, the simplest oxidation reaction, i.e., CO oxidation, was employed as the model reaction to establish a basis of the reactivity of Cd(I) in zeolite. Researches on the reactivity toward other molecules including ethylene and olefins are also valuable to understand the behavior of Cd(I) as the reactive center. Further exploring the reactivity toward ethylene and olefin, which is more challenging to be achieved due to the rich varieties of reaction routes, byproducts, and products in this zeolite system, is ongoing in our laboratory.

(38) J. Li, M. Hermann, G. Frenking and C. Jones, *Angew. Chem. Int. Ed.* 2012, **51**, 8611–8614.

For Table of Contents Only



We report on a new functionality of cadmium created by zeolite lattice: room temperature O transfer from N₂O to CO mediated by nearest monovalent cadmium ions in MFI zeolite. To our knowledge, this is the first example regarding to reversible reactivity of nearest Cd^I species toward stable small molecules. The experimentally calibrated DFT calculations showed that charge compensation requirements from the nearest two Al sites arrayed circumferentially in the 10-membered ring of MFI zeolite creates such reversible reactivity of Cd^I. The unprecedented reactivity of Cd^I and its origin are discussed.